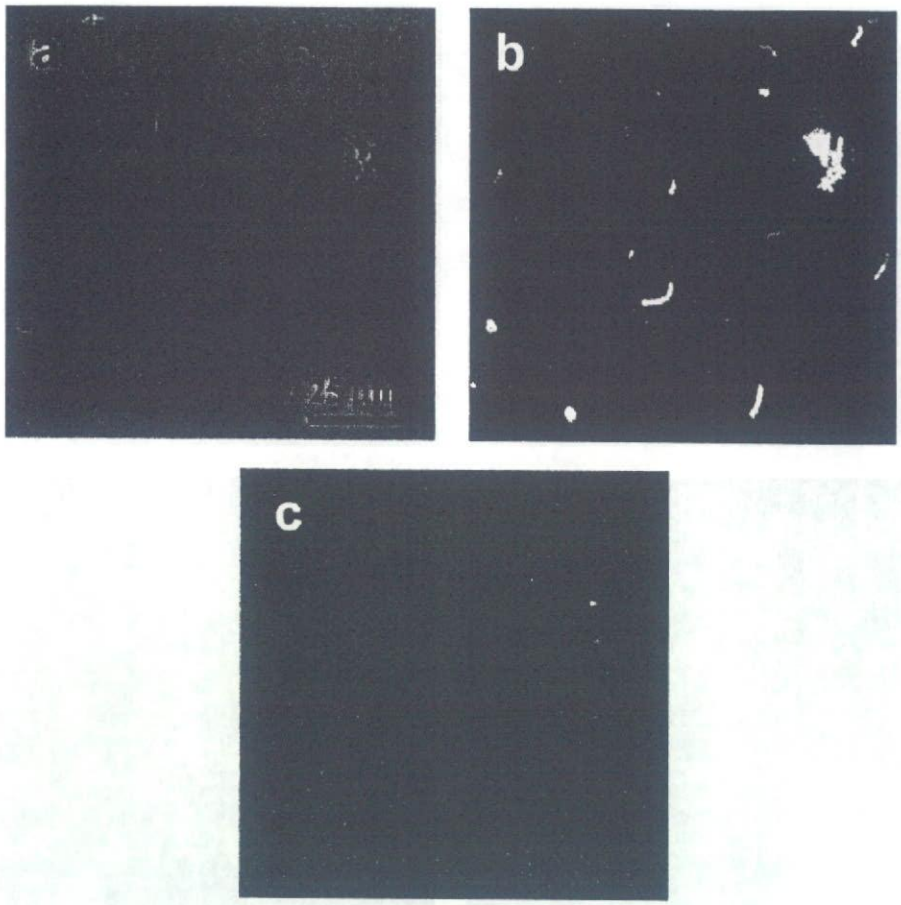

Figure 5. CLSM images of the 200-MWNTs coated with FITC-PVLA after incubation with Rhod-ConA. (a) Transmitted light channel, (b) FITC channel, and (c) Rhodamine channel.

adsorbed on the MWNTs are recognized specifically by β-galactose-specific RCA_{120} lectin (36).

However, certain proteins were found to bind to CNTs via hydrophobic interactions even without sidewall functionalization (9, 11). To determine the nonspecific binding of lectins as a control experiment, bare MWNTs were incubated with lectins. Nonspecific bindings of lectins were observed as shown in Figure 6, in which CLSM images show adsorbed lectins on bare MWNTs. Binding of lectins to CNTs could also be driven by hydrophobic interactions.

On the basis of our experimental results, it was thought that the interaction between the MWNTs coated with PVLA and RCA_{120} was specific and not due to a variation in physical adsorption, since ConA did not interact with the coated MWNTs. This also indicated that the entire hydrophobic area on the surface of the MWNTs was coated and blocked with PVLA.

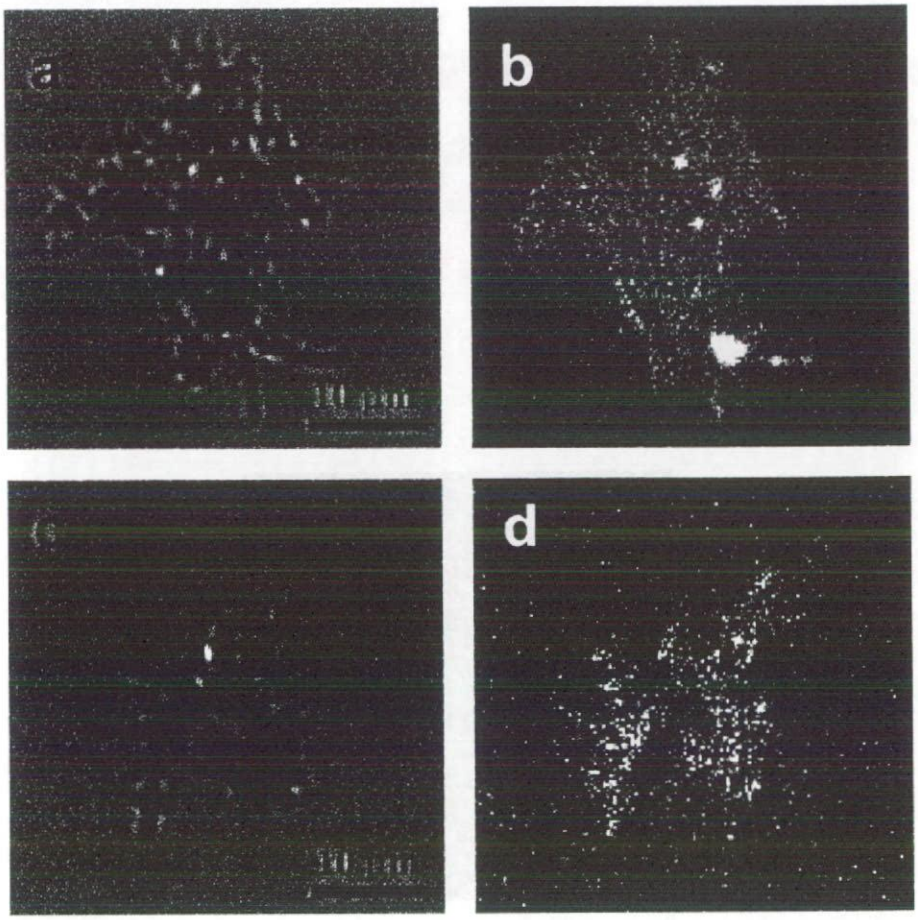

Figure 6. CLSM images of bare 200-MWNTs after incubation with Rhod-RCA_{120} (upper) and Rhod-ConA (lower). (a, c) Transmitted light channel, (b, d) Rhodamine channel.

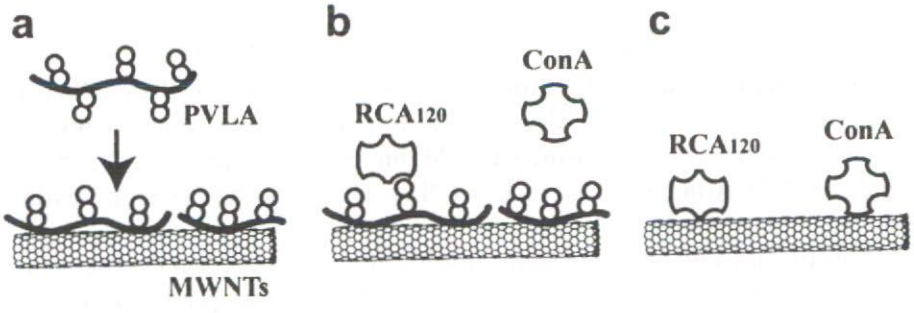

Scheme 1. Illustrations of (a) adsorption of PVLA onto the surface of MWNTs, (b) specific interaction between the MWNTs coated with PVLA and lectins, and (c) non-specific interaction between MWNTs and lectins.

CONCLUSION

In summary, we have demonstrated that the MWNTs coated with a carbohydrate-carrying polymer for use as biological recognition signals can be easily prepared by a non-covalent method via hydrophobic interactions (Scheme 1). The MWNTs coated with a carbohydrate-carrying polymer were found to acquire a selective binding affinity to the corresponding lectin. Modification of CNTs with various carbohydrate chains will be a useful protocol for molecular designs of biomaterials, nanoarchitecture, and biosensors.

ACKNOWLEDGMENTS

We would like to thank Dr. Yoshinori Sato and Prof. Kazuyuki Tohji, Graduate School of Environmental Studies, University of Tohoku, for providing carbon nanotubes and for their helpful discussions. This study was supported by Health and Labor Science Research grants in 2006 (H18-kagaku-006) from the Ministry of Health, Labor and Welfare of Japan. Part of this work was also supported by a Grant-in-Aid for Scientific Research (No. 16791177) from the Ministry of Education, Culture, Sports, Science, and Technology of Japan.

REFERENCES

1. Balasubramanian, K. and Burghard, M. (2005) Chemically functionalized carbon nanotubes. *Small*, 1: 180.
2. Hirsch, A. (2002) Functionalization of single-walled carbon nanotubes. *Angew. Chem. Int. Ed.*, 41: 1853.
3. Bahr, J.L. and Tour, J.M. (2002) Covalent chemistry of single-wall carbon nanotubes. *J. Mater. Chem.*, 12: 1952.
4. Khabashesku, V., Billups, W.E., and Margrave, J.L. (2002) Fluorination of single-wall carbon nanotubes and subsequent derivatization reactions. *Acc. Chem. Res.*, 35: 1087.
5. Sun, Y.P., Fu, K., Lin, Y., and Huang, W. (2002) Functionalization of carbon nanotubes: properties and applications. *Acc. Chem. Res.*, 35: 1096.
6. Niyogi, S., Hamon, M.A., Hu, H., Zhao, B., Bhowmik, P., Sen, R., Itkis, M.E., and Haddon, R.C. (2002) Chemistry of single-walled carbon nanotubes. *Acc. Chem. Res.*, 35: 1105.
7. Guo, Z., Sadler, P.J., and Tsang, S.C. (1998) Immobilization and visualization of DNA and proteins on carbon nanotubes. *Adv. Mater.*, 10: 701.
8. Hazani, M., Naaman, R., Hennrich, F., and Kappes, M.M. (2003) Confocal fluorescence imaging of DNA-functionalized carbon nanotubes. *Nano Lett.*, 3: 153.
9. Balavoine, F., Schultz, P., Richard, C., Mallouh, V., Ebbesen, T.W., and Mioskowski, C. (1999) Helical crystallization of proteins on carbon nanotubes:

a first step towards the development of new biosensors. *Angew. Chem. Int. Ed.*, 38: 1912.
10. Huang, W., Taylor, S., Fu, K., Lin, Y., Zhang, D., Hanks, T.W., Rao, A.M., and Sun, Y.P. (2002) Attaching proteins to carbon nanotubes via diimide-activated amidation. *Nano Lett.*, 2: 311.
11. Zhao, Y.D., Zhang, W.D., Chen, H., and Luo, Q.M. (2002) Direct electron transfer of glucose oxidase molecules adsorbed onto carbon nanotube powder microelectrode. *Anal. Sci.*, 18: 939.
12. Davis, J.J., Green, M.L.H., Hill, H.A.O., Leung, Y.C., Sadler, P.J., Sloan, J., Xavier, A.V., and Tsang, S.C. (1998) The immobilization of proteins in carbon nanotubes. *Inor. Chim. Acta.*, 272: 261.
13. Nimmagadda, A., Thurston, K., Nollert, M.U., and McFetridge, P.S. (2006) Chemical modification of SWNT alters *in vitro* cell-SWNT interactions. *J. Biomed. Mater. Res. A*, 76: 614.
14. Star, A., Steuerman, D.W., Heath, J.R., and Stoddart, J.F. (2002) Starched carbon nanotubes. *Angew. Chem. Int. Ed.*, 41: 2508.
15. Lii, C.Y., Stobinski, L., Tomasik, P., and Liao, C.D. (2003) Single-walled carbon nanotube-poteto amylose complex. *Carbohydr. Polym.*, 51: 93.
16. Bandyopadhyaya, R., Nativ-Roth, E., Regev, O., and Yerushalmi-Rozen, R. (2002) Stabilization of individual carbon nanotubes in aqueous solutions. *Nano Lett.*, 2: 25.
17. Stobinski, L., Tomasik, P., Lii, C.Y., Chan, H.H., Lin, H.M., Liu, H.L., Kao, C.T., and Lu, K.S. (2003) Single-walled carbon nanotube-amylopectin complexes. *Carbohydr. Polym.*, 51: 311.
18. Chambers, G., Carroll, C., Farrell, G.F., Dalton, A.B., McNamara, M., in het Pahuis, M., and Byrne, H.J. (2003) Characterization of the interaction of gamma cyclodextrin with single-walled carbon nanotubes. *Nano Lett.*, 3: 843.
19. Shin, M., Kam, N.W.S., Chen, R.J., Li, Y., and Dai, H. (2002) Functionalization of carbon nanotubes for biocompatibility and biomolecular recognition. *Nano Lett.*, 2: 285.
20. Mattson, M.P., Haddon, R.C., and Rao, A.M. (2000) Molecular functionalization of carbon nanotubes and use as substrates for neuronal growth. *J. Mol. Neurosci.*, 14: 175.
21. Fukuda, M. and Hindsgaul, O. (eds.) (1994) *Molecular Glycobiology*; IRL: Oxford.
22. Lee, Y.C. and Lee, R.T. (eds.) (1994) *Neoglycoconjugates: Preparation and Applications*; Academic Press: San Diego, CA.
23. Bovin, N.V. (1998) Polyacrylamide-based glycoconjugates as tools in glycobiology. *Glycoconj. J.*, 15: 431.
24. Rye, P.D. and Bovin, N.V. (1997) Selection of carbohydrate-binding cell phenotypes using oligosaccharide-coated magnetic particles. *Glycobiology*, 17: 179.
25. Choi, S.K., Mammen, M., and Whitesides, G.M. (1997) Generation and in situ evaluation of libraries of poly(acrylic acid) presenting sialosides as side chains as polyvalent inhibitions of influenza-mediated hemagglutination. *J. Am. Chem. Soc.*, 119: 4103.
26. Lees, W.J., Spaltenstein, A., Kingery-Wood, J.E., and Whitesides, G.M. (1994) Polyacrylamides bearing pendant α-sialoside groups strongly inhibit agglutination of erythrocytes by influenza A virus: multivalency and steric stabilization of particulate biological systems. *J. Med. Chem.*, 37: 3419.
27. Sakamoto, J., Koyama, T., Miyamoto, D., Yingsakmongkon, S., Hidari, K.I., Jampangern, W., Suzuki, T., Suzuki, Y., Esumi, Y., Hatano, K., Terunuma, D.,

and Matsuoka, K. (2007) Thiosialoside clusters using carbosilane dendrimer core scaffolds as a new class of influenza neuraminidase inhibitors. *Bioorg. Med. Chem. Lett.*, 17: 717.

28. Lee, Y.C. and Lee, R.T. (1995) Carbohydrate-protein interactions: basis of glycobiology. *Acc. Chem. Res.*, 28: 321–7.
29. Page, D. and Roy, R. (1997) Optimizing lectin-carbohydrate interactions: improved binding of divalent α-mannosylated ligands towards concanavalin A. *Glycoconj. J.*, 14: 345.
30. Page, D., Zanini, D., and Roy, R. (1996) Macromolecular recognition: effect of multivalency in the inhibition of binding of yeast mannan to concanavalin A and pea lectins by mannosylated dendrimers. *Bioorg. Med. Chem.*, 4: 1949.
31. Kobayashi, K. and Sumitomo, H. (1987) Synthesis and functions of polystyrene derivatives having pendant oligosaccharides. *Polym. J.*, 17: 567.
32. Hoshiba, T., Nagahara, H., Cho, C.S., Tagawa, Y., and Akaike, T. (2007) Primary hepatocyte survival on non-integrin-recognizable matrices without the activation of Akt signaling. *Biomaterials*, 28: 1093.
33. Cho, C.S., Kobayashi, A., Takei, R., Ishihara, T., Maruyama, A., and Akaike, T. (2001) Receptor-mediated cell modulator delivery to hepatocyte using nanoparticles coated with carbohydrate-carrying polymers. *Biomaterials*, 22: 45.
34. O'Connell, M.J., Boul, P., Ericson, L.M., Huffman, C., Wang, Y., Haroz, E., Kuper, C., Tour, J., Ausman, K.D., and Smalley, R.E. (2001) Reversible water-solubilization of single-walled carbon nanotubes by polymer wrapping. *Chem. Phys. Lett.*, 342: 265.
35. Price, R.L., Ellison, K., Haberstroh, K.M., and Webster, T.J. (2004) Nanometer surface roughness increases select osteoblast adhesion on carbon nanofiber compacts. *J. Biomed. Mater. Res. A*, 70: 129.
36. Chevolot, Y., Martins, J., Milosevic, N., Leonard, D., Zeng, S., Malissard, M., Berger, E.G., Maier, P., Mathieu, H.J., Crout, D.H.G., and Sigrist, H. (2001) Immobilization on polystyrene of diazirine derivatives of mono- and disaccharides: biological activities of modified surfaces. *Bioorg. Med. Chem.*, 9: 2943.

Available online at www.sciencedirect.com
ScienceDirect
Applied Surface Science 254 (2007) 621–626
applied surface science
www.elsevier.com/locate/apsusc

Positioning of cationic silver nanoparticle by using AFM lithography and electrostatic interaction

Tetsu Yonezawa [a,b,*], Tetsuya Itoh [a], Naoto Shirahata [a,c], Yoshitake Masuda [a,d], Kunihito Koumoto [a]

[a] Department of Applied Chemistry, Graduate School of Engineering, Nagoya University, Furo-cho, Chikusa, Nagoya 464-8603, Japan
[b] Department of Chemistry, Graduate School of Science, The University of Tokyo, Bunkyo, Tokyo 113-0033, Japan
[c] Fine Particle Processing Laboratory, Materials Engineering Laboratory (MEL), National Institute for Materials Science (NIMS), 1-2-1 Sengen, Tsukuba 305-0047, Japan
[d] National Institute of Advanced Industrial Science and Technology (AIST), 2266-98 Anagahora, Shimo-shidami, Moriyama, Nagoya 463-8560, Japan

Received 23 October 2006; received in revised form 11 April 2007; accepted 25 June 2007
Available online 28 June 2007

Abstract

One-dimensional metal lines of silver nanoparticles with a nano-sized width were generated onto silicon surface by using a nano-level lithography technique, field induced oxidation (FIO) by AFM, on self-assembled monolayer-modified Si wafers. This FIO technique provided SiO_2 lines a width of less than 100 nm. Short-time immersion of partially anodized silicon surface which is covered by a cationic silanol surfactant ($((CH_3O)_3SiCH_2CH_2CH_2N(CH_3)_3{}^+Cl^-$)-monolayer into quaternary ammonium ($HSCH_2CH_2N(CH_3)_3{}^+Br^-$)-covered silver nanoparticles readily and reproducibly gave nano-metal lines of silver onto silicon wafers. Hydrophilicity of the whole wafer surface was indispensable for homogeneously wetting the anodized SiO_2 area with a nanodimensional width.

PACS : 81.16.Dn; 68.37.Ps

Keywords: Nanoparticle; Silver; Monolayer; AFM

1. Introduction

Nanoparticles have been more and more intensively investigated as one of key materials of recent nanotechnology, catalysis, and biochemistry [1–3]. Especially, well-controllable nanostructures with low dimension on a substrate play a central role in the development of actual nanotechnology [4]. Self-organization or self-assembly techniques of nano-sized materials is intensively investigated for constructing such nanostructures. However, most of the self-organized structures of metal nanoparticles without templates are in two- or three-dimension. Metal one-dimensional arrays, which can be called as "nanowires", have been reported by using various templates [5], special stabilizing reagents [6], or lithography [7]. Both soft templates, such as DNA, polymers and other organic molecules, and hard templates, such as micropore inorganic materials or crystals, are used. Such template systems for preparation of metal nanowires can be largely divided into two categories. One is the arrangement of metal nanoparticles in one dimension by using some temperates. The other one is direct preparation of metal nano-wires by reducing metal ions on templates. We and others used DNA molecules as soft templates for arrangement of cationic metal nanoparticles. Some solid templates, such as mesopore type metal oxides [8], can also be used for 1D arrangement of metal nanoparticles. Direct preparation method with DNA molecules as soft templates has been also proposed for Ag or Pd nanowires. Adsorption of metal cations (for example, Ag^+ or Pd^{2+}) on DNA molecules followed by reduction gave one-dimensional nanowires of the corresponding metals [9,10]. In Table 1, various preparative processes of one-dimensional metal nanoparticle arrays and metal nanowires with nanodimensional widths by using organic or inorganic templates are listed [11–24].

* Corresponding author at: Department of Chemistry, Graduate School of Science, The University of Tokyo, Bunkyo, Tokyo 113-0033, Japan.
E-mail address: tetsu@chem.s.u-tokyo.ac.jp (T. Yonezawa).

0169-4332/$ – see front matter © 2007 Elsevier B.V. All rights reserved.
doi:10.1016/j.apsusc.2007.06.046

Table 1
Various preparative procedures of one-dimensional assembly of nanoparticles and nanowires with various templates

Metal	Template	Assembly formation	Ref. nos.
Au	DNA/RNA	Electrostatic interaction	[5,11–15]
Au	TMV	Electrostatic interaction	[16]
Pd	DNA	Electrostatic interaction	[17]
Ag, Cu, Pt, Pd, Au	DNA	Metallization	[9,10,18–20]
Au	Mesoporous Al_2O_3	Evaporation	[8]
Au	Nanoshaving	Evaporation	[22]
Au	Dendron ligands	Evaporation	[6]
Au	Carbon step edge	Evaporation	[23]
Au	Surface activation	Dipping	[24]
Au	Lithography	LB	[3]
Pt	Mesoporous SiO_2	Metallization	[21]

Nano-lithography on flat substrates has been also useful to construct one-dimensional metal nanoparticle assemblies. Scanning probe lithography or drawing with self-assembled monolayers has a high ability to organize materials on the nanometer scale [25]. Dip-pen technology is useful to draw one-dimensional nanoparticle arrays. On the other hand, anodic nano-oxidation by using an AFM probe is useful to provide SiO_2 structures on Si substrates in nanometer order. With this technique, one can also remove SAM molecules selectively and generate SiO_2 selectively, which was proposed by Sugimura and Nakagiri [26] Recently, Liu and coworkers followed Sugimura's approach and proposed the preparation of nanopatterned assembling of gold nanoparticles onto an amine-terminated SAM surface which was selectively oxidized by AFM [27]. However, such coordinative ligand adsorption of metal nanoparticles could not have densely packed nanoparticle structures and this process should have taken very long immersion time (12 h). Furthermore, smaller patterns showed lower efficiency for adsorption of nanoparticles [28]. Therefore, alternative approaches should be proposed.

On the other hand, densely-packed patterning of submicron-sized spherical particles by using patterning of SAM on silicon substrates was successfully carried out. Particle wires with a micron-width could be obtained on a silanol/alkyl patterned surface generated by UV-lithography [29]. But wetting behavior can be different on submicron (or smaller)-sized patterns. Therefore, more precisely designed molecular temperates should be proposed.

This paper reports the fabrication of 1D silver nanoparticle arrays by simple immersion of AFM-modified Si surface covered by cationic SAM into an aqueous dispersion of cationic Ag nanoparticles. AFM-modification of Si, that is, field induced oxidation (FIO) by AFM is a system of anodic oxidation of silicon by using conductive AFM cantilevers as negative electrodes. As for the monolayer on silicon substrate, we have used alkyl (hydrophobic)-SAM and quaternary ammonium (hydrophilic/cationic)-SAM. For nanosized patterns, hydrophilic monolayer may be useful to obtain better particulate structures. As SiO_2 nanolines are negatively charged at ambient conditions [30], they can densely adsorb Ag nanoparticles with highly positively charged surface.

2. Experimental

Water was purified by a Mili-Q system (>18 MΩ). Thiocholine bromide (TCBr, $HS(CH_2)_2N(CH_3)_3^+Br^-$), which was used as the stabilizer reagent in this study, was obtained by hydrolysis of acetylthiocholine bromide (Aldrich or ACROS) [5]. Its purity was checked by ^1H NMR, FT-IR and elemental analysis. Other chemicals were used as received. Silver nanoparticles used here were produced by chemical reduction from AgCl according to the preparative method reported previously [31]. The nanoparticles were then purified by re-precipitation and centrifugation in order to exclude the excess unbounded stabilizer molecules and the residue of the reducing reagent. Purified Ag nanoparticles were re-dispersed into water (Fig. 1).

Silicon wafers were purchased from Chiyoda Corporation: P-type Si (1 0 0) wafers with a resistivity in the range of 5–10 Ω cm. The substrates were first put into UV-ozone substrate cleaner (Filgen Co., Japan) in order to remove organic contamination on the substrate surface, and then degreased ultrasonically in toluene, ethanol, and water. They were then immersed into a conc. HCl/CH_3OH (1:1, v/v) for 30 min, and conc. H_2SO_4 for 30 min. Again the wafers were washed by water and then immersed into boiling water for 10 min. After removing water by washing with acetone, the cleaned wafers were kept in acetone until use.

For the preparation of self-assembled monolayer (SAM) on silicon surface, trimethoxysilyl-*n*-propyl-*N*,*N*,*N*-trimethylammonium chloride (TTCl, Gelest, Inc., 50% in methanol) and *n*-octyltrichlorosilane (OTS, Azmax Co.) were selected to obtain hydrophilic and hydrophobic surfaces on a silicon wafer, respectively. The reaction was carried out under dried nitrogen atmosphere in order to avoid hydrolysis of the

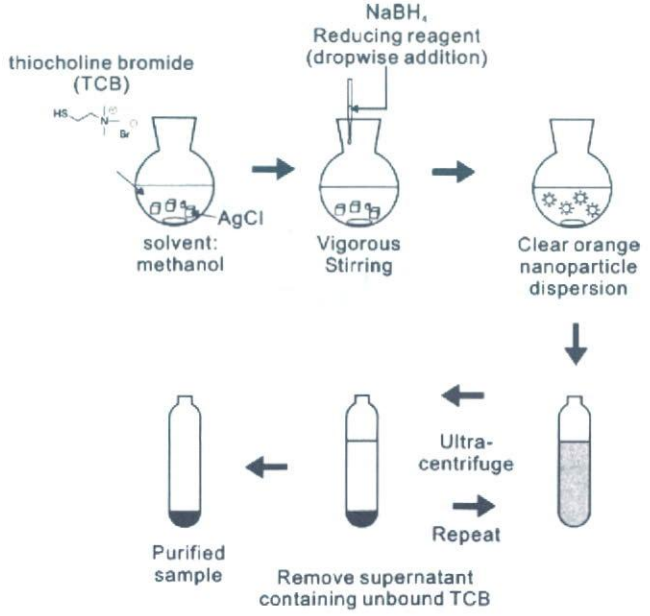

Fig. 1. Schematic illustration of preparation and purification of cationic Ag nanoparticles stabilized by thiocholine bromide.

reagents. Silane-coupling reagents react quite rapidly with water molecules in air. Into the methanol solution of TTCl (10 vol%) or a toluene solution of OTS (10 vol%), freshly cleaned silicon wafers were immersed for ca. 5 min under dry nitrogen atomosphere. The wafers were washed by the corresponding solvent for excess unbound SAM reagents and dried. The modified wafers were then put into an oven at 120 °C for 5 min in order to complete silane-coupling reaction. Finally, the surface was rinsed carefully with pure water several times.

Field induced oxidation (FIO) by AFM is a system of anodic oxidation of silicon by using conductive AFM cantilevers as negative electrodes. With the self-assembled monolayers on silicon, FIO removes organic monolayers and changes Si surface to SiO_2. This system, therefore, can work as nano-lithography on silicon surface. The AFM system used here is a set of a Seiko Instrument SPI-3800N probe station. AFM nano-oxidation of SAM-covered silicon surface was conducted with a gold-coated AFM probe (Seiko Instrument: SI-AF01-A) in contact mode. The injection voltage used was 7 V and the scanning speed was 0.1 $\mu m\ s^{-1}$.

The preparation scheme of nanoparticle wires is illustrated in Fig. 2. After field-induced oxidation (FIO) by AFM, modified substrates were immersed for 1 min into the aqueous dispersion of TCBr-stabilized Ag nanoparticles (10 wt%) in order to deposit nanoparticles on SiO_2 area which is hydrophilic and is slightly negatively charged at ambient conditions. When silica surface contacts with water, silanol groups (Si–OH) are generated. At ambient conditions, silanol groups are ionized as $Si–O^-$ and the surface is negatively charged [30]. After immersion, the substrate was blown by nitrogen flow, and was immersed into ethanol for fixation. The sample was then kept at 120 °C for 5 min and then rinsed by pure water.

3. Results and discussion

Cationic silver nanoparticles used here were prepared from insoluble metal source, AgCl by using $NaBH_4$ as the reducing reagent [31]. Under vigorous stirring, after injection of aq. $NaBH_4$ by using a syringe pump for dropwise injection, the colorless liquid containing AgCl powders gradually changed to a brown and homogeneous dispersion, which indicates the formation of the silver nanoparticles. No aggregate or precipitate was observed for several days. In order to remove excess stabilizing reagent and by-products, ultracentrifugation (Hitachi GX-150) was used. Excess stabilizing reagents, that is, unbound thiocholine bromide molecules, strongly prohibit the adsorption of particles on anionic sites. The nanoparticle dispersions were washed and ultra-centrifuged three times in order to remove out the unbound thiocholine bromide molecules, and concentrated into 10 mg cm^{-3} of the concentration of Ag atoms. The particles were highly spherical and uniform. The average diameter of the metal core of obtained Ag nanoparticles was 6.7 nm as described before [31]. The concentrated particle dispersion was also enough stable.

There are several techniques to prepare self-assembled monolayers on silicon surface, such as simple dip into a silane or silanol solution [32], vacuum evaporation or plasma CVD of

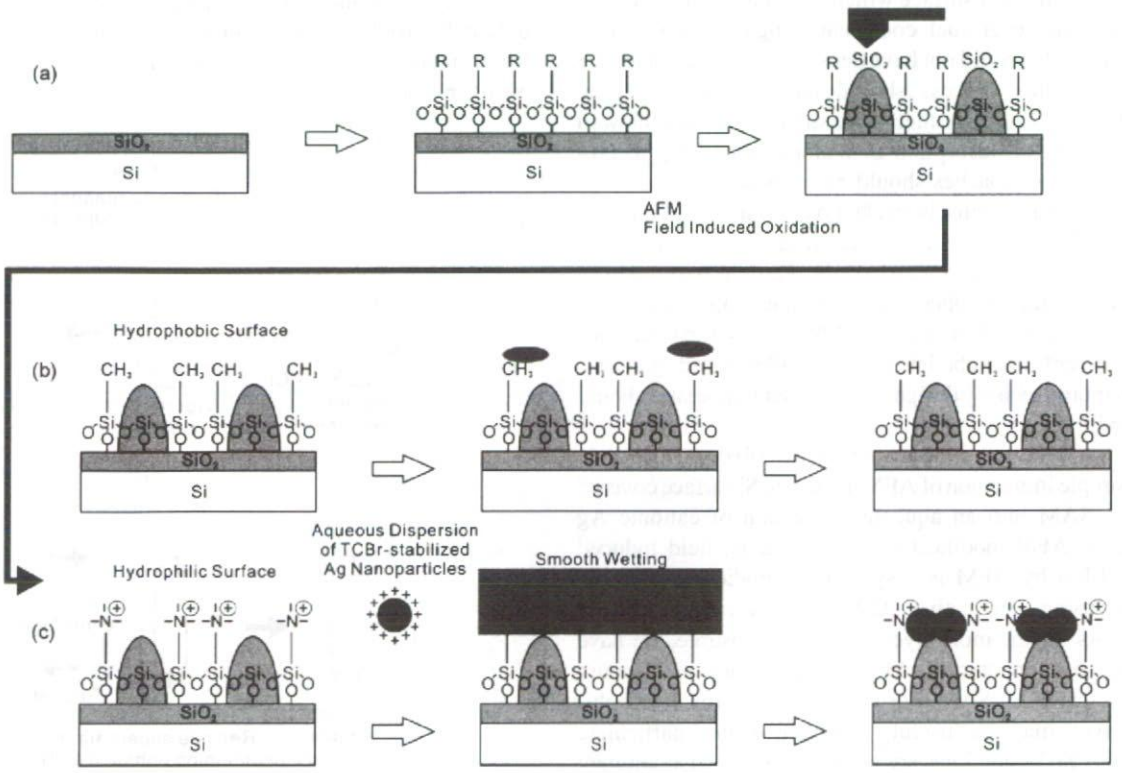

Fig. 2. Schematic illustration of FIO (field induced oxidation) lithography with a scanning probe (a). Immobilization of cationic Ag nanoparticles onto oxide area prepared on (b) OTS-SAM or (c) TTCl-SAM.

silane-coupling reagents [33] as well as alkyl monolayer via Si–C covalent bonds obtained by hydrosilylation [34]. For preparation of stable and reproducible SAMs, we have selected the simple immersion method, which was followed by annealing. This method does not need any special expensive apparatuses or vacuum systems. Formation of SAMs on silicon surface was checked by water contact angle measurement on the SAM-coated surface. OTS-SAM surface became more hydrophobic and its water contact angle was 96°. On the contrary, TTCl-SAM surface changed much hydrophilic and it showed less than 5° of its water contact angle. Quaternary ammonium halides are ionized at any pH conditions and TTCl-SAM generates a cationic and hydrophilic surface. These values suggest the formation of monolayer which fully covered the silicon surface by silane-coupling reaction. No obvious degradation of SAM was found for several days under clean and dry atmosphere.

FIO by AFM could be applied on the both of the OTS- and TTCl-SAM coated silicon wafers. The width and thickness of oxidized SiO_2 lines can be varied with the filed voltage and the scanning speed of the AFM probe [29]. With an injection voltage of 7 V and a scanning speed of 0.1 μm s^{-1}, the width of the SiO_2 nanowire obtained here was ca. 80 nm and the width of the most area was less than 100 nm. Fig. 3a shows an AFM image of FIO scanned lines on a TTCl-SAM coated Si wafer.

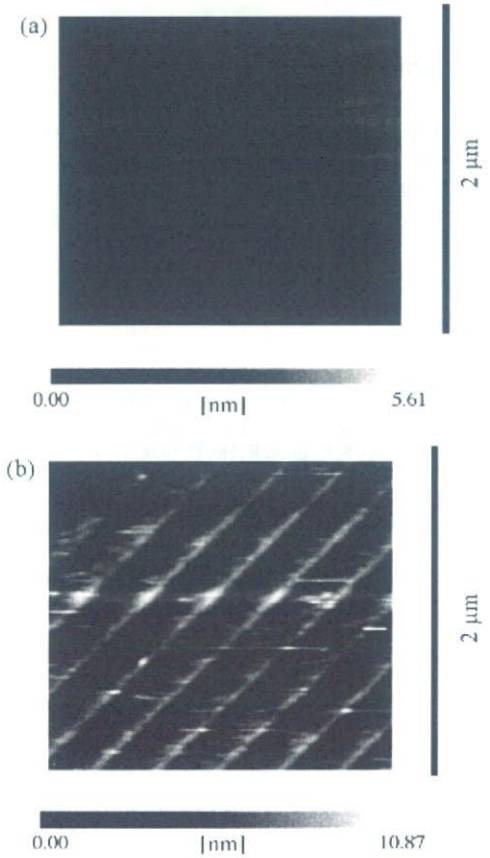

Fig. 3. AFM images of (a) the nanoline patterns prepared on a Si wafer covered by TTCl-SAM and (b) the modified nanolines on the TTCl-SAM coated silicon wafer after immersion into Ag nanoparticle dispersion.

Owing to the volume expansion, which accompanied with the anodation of the Si substrate to SiO_2, the probe-scanned area is slightly higher than the surrounding unscanned areas. TTCl molecules in the scanned area were removed out during oxidation, therefore, nanoline area is negatively charged at ambient condition. The water drop contact angle on SiO_2 generated by photo-etching of SAM on silicon wafer was ~5° [32], which indicates that SiO_2 area is hydrophilic.

After FIO treatment, the modified TTCl-SAM and OTS-SAM coated Si substrates were then immersed into the aqueous dispersions of cationic Ag nanoparticles, which were surrounded by thiocholine bromide and were highly positively charged. Ag nanoparticles were stable enough even after purification and no precipitates were observed in the dispersion. The modified wafers were then rinsed by water for several times and sonicated in water in order to remove physical adsorbed silver nanoparticles. The results of absorption of Ag nanoparticles on the two modified substrates were different.

On the modified OTS-SAM coated Si wafer, unfortunately, no good image which indicated the deposition of the silver nanoparticles on the oxidized area was obtained, even SiO_2 surface was negatively charged at ambient conditions. This can probably be attributed to the fact that the aqueous dispersion of nanoparticles could not well wet the OTS-SAM coated Si substrate according to the hydrophobicity of the OTS surface. Even though this FIO process removes hydrophobic OTS-SAM area to SiO_2 surface and that nanolines are hydrophilic, when the hydrophilic area, surrounded by the hydrophobic area, is too small, the drops of the aqueous dispersion could not reach the hydrophilic surface (Fig. 2b). In that case, according to this low wettability on SiO_2 nanolines generated by FIO, no electrostatic nanoparticle deposition can be observed even the particle surface is highly positively charged.

As the alternative possibility, we have chosen TTCl-SAM coated Si substrates for one-dimensional nanoparticle assembly. This surface is highly hydrophilic (water contact angle <5°) and highly positively charged because the surface of Si is fully covered by quaternary ammonium chloride groups. As described above, SiO_2 area generated by FIO process is negatively charged and was surrounded by highly cationic surface, which is also hydrophilic. Therefore, if the aqueous dispersion of cationic nanoparticles wets the substrate surface very well, the positively charged Ag nanoparticles must be electrostatically deposited selectively onto the SiO_2 area (Fig. 2c). Once deposited on SiO_2 area, inter-ionic force induces densely-packed nanoparticle structures. Densely-packed 1D arrays of TCBr-stabilized metal nanoparticles could also be obtained on DNA bundles [5,11–15,17]. The AFM image of the nanoparticle adsorbed surface is shown in Fig. 3b. The average height of the nanowires is ca. 3.6 nm, which is 2.8 nm higher than that of the nano-lines of SiO_2 prepared by FIO process (ca. 0.8 nm, Fig. 3a). This value is smaller than the average size of silver cationic nanoparticles (=6.7 nm [31]). But according to the annealing at 120 °C after immersion, densely adsorbed small-ligand stabilized silver nanoparticles with the size of single nanometer should be sintered. For example, gold nanoparticles stabilized also by

TCBr were immediately fused even at room temperature when they were densely accumulated on DNA bundles [5]. In general, during the sintering process of the monolayer of silver nanoparticles, the material experiences significant densification with shrinkage.

Comparing with the reported system [27], that is, adsorption of bare gold nanoparticles on amine-terminated SAM lines (12 h), this process needed very short immersion time (1 min). This indicates that self-assembly by using electrostatic interaction is very rapid process, and the cationic nanoparticles are immediately adsorbed on the anionic SiO_2 lines. In the case of such a very short process, the wettability of the dispersion on the surface is highly important.

In order to confirm the selective adsorption and positioning of Ag nanoparticles onto the modified SiO_2 surface, X-ray photospectrcopic (XPS) measurements were carried out. However, it was impossible, unfortunately, to detect the Ag signals on FIO modified substrates because the area modified by an AFM-probe was too small. Therefore, in this study, two typical substrates were used for XPS measurements, for this purpose. A TTCl-coated Si substrate and a native Si substrate which was covered by SiO_2 were immersed into the Ag nanoparticle dispersion. Then, XPS spectra were obtained. In Fig. 4, XPS spectra of both the surfaces are collected. On SiO_2 surface, strong Ag peaks can be observed at 369 eV and 375 eV, which are corresponding to $3d_{5/2}$ and $3d_{3/2}$, respectively. On the contrary, only small peaks are found on TTCl-coated Si surface. These two XPS spectra strongly support the AFM results observed in Fig. 3b, that is cationic Ag nanoparticles were adsorbed selectively on SiO_2 nanolines generated by FIO modification.

Advantage of the simple immersion method to generate one-dimensional nanoparticle arrays reported here is the versatility and easiness of working in aqueous dispersions of nanoparticles and under ambient condition. High area selectivity was also observed, because nanoparticles do not deposit on areas of TTCl-SAM according to the positive–positive charge repulsion. For the formation of narrow 1D nanoparticle arrays with several 10 mm width and a very short immersion time, wettability of nanoparticle dispersions on the substrate is highly important. As water could not wet SiO_2 surface prepared on hydrophobic OTS-SAM layered silicon surface, no nanoparticle adsorption was observed.

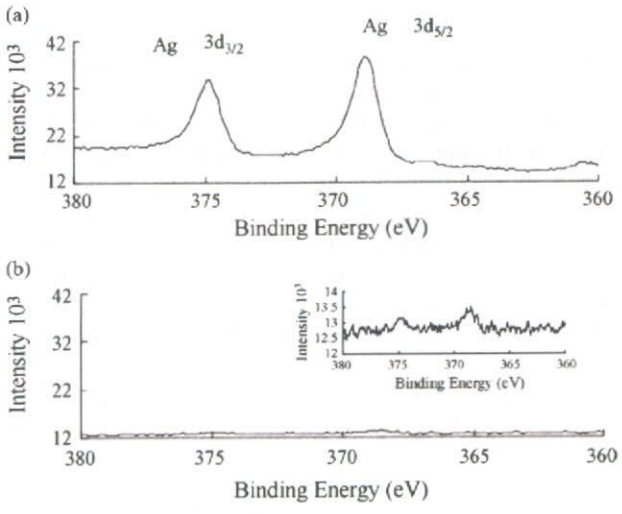

Fig. 4. X-ray photospectroscopic spectra of (a) Si–OH covered Si surface and (b) TTCl-SAM covered Si surface after their immersion into the dispersion of cationic Ag nanoparticles. Inset of (b), enlarged image.

4. Conclusion

One-dimensional nanoparticle arrays with the width of less than 100 nm could be generated by simple immersion of silicon substrate covered by quaternary ammonium groups. Wettability of the nanoparticle dispersions on the substrate surface is highly important for immobilization of nanoparticles. FIO-modified SiO_2 area are is hydrophilic and anionic but when this area is very small and surrounded by hydrophobic surface, that is, the OTS-covered surface, the aqueous drops containing the silver nanoparticles cannot wet the FIO-modified part. Then, nanoparticle assemblies in nanosized area cannot be achieved. On the contrary, FIO-modified SiO_2 surface could adsorb Ag nanoparticles densely when the surface was covered by hydrophilic TTCl-SAM. Such hydrophilic monolayer surface may be useful for preparing good nanoparticle structures in nano-dimension, which is difficult on alkyl-type monolayer surface.

Acknowledgements

This work is partly supported by a Grant-in-Aid from the Japan Society for the Promotion of Science (JSPS). NS acknowledges the post-doctoral fellowship from JSPS. TY thanks the warm hospitality of Prof. H. Nishihara (Univ. Tokyo).

References

[1] G. Schmid (Ed.), Nanoparticles, Wiley-VCH, Weinheim, 2004.
[2] T. Yonezawa, N. Toshima, New J. Chem. (1998) 1179–1201.
[3] M.-C. Daniel, D. Astruc, Chem. Rev. 104 (2004) 293–346.
[4] J. Huang, A.R. Tao, S. Connor, R. He, P. Yang, Nano Lett. 6 (2006) 524–529.
[5] T. Yonezawa, S. Onoue, N. Kimizuka, Chem. Lett. (2002) 1172–1173.
[6] S. Nakao, K. Torigoe, K. Kon-no, T. Yonezawa, J. Phys. Chem. B 106 (2002) 12097–12100.
[7] P.M. Mendes, S. Jacke, K. Critchley, J. Plaza, Y. Chen, K. Nikitin, R.E. Palmer, J.A. Preece, S.D. Evans, D. Fitzmaurice, Langmuir 20 (2004) 3766–3768.
[8] G. Hornyak, M. Kröll, R. Pugin, T. Sawitowski, G. Schmid, J.-O. Bovin, G. Karsson, H. Hofmeister, S. Hopfe, Chem. Eur. J. 3 (1997) 1951–1956.
[9] E. Braun, Y. Eichen, U. Sivan, G. Ben-Yoseph, Nature 391 (1998) 775–778.
[10] J. Richter, R. Seidel, R. Kirsch, M. Mertig, W. Pompe, J. Plaschke, H.K. Schackert, Adv. Mater. 12 (2000) 507.
[11] T. Yonezawa, S. Onoue, T. Kunitake, Kobunshi Ronbunshu 56 (1999) 855.
[12] M.G. Warner, J.E. Hutchison, Nat. Mater. 2 (2003) 232.
[13] A.Y. Koyfman, G. Braun, S. Magonov, A. Chworos, N.O. Reich, L. Jaeger, J. Am. Chem. Soc. 127 (2005) 11886–11887.
[14] G.H. Woehrle, M.G. Warner, J.E. Hutchison, Langmuir 20 (2004) 5982–5988.

[15] G. Braun, K. Inagaki, R.A. Estabrook, D.K. Wood, E. Levy, A.N. Cleland, G.F. Strouse, N.O. Reich, Langmuir 21 (2005) 10699–10701.
[16] T. Yonezawa, S. Onoue, N. Kimizuka, Chem. Lett. 34 (2005) 1498–1499.
[17] M. Hosogi, G. Hashiguchi, M. Haga, T. Yonezawa, K. Kakushima, H. Fujita, Jpn. J. Appl. Phys. 44 (2005) L955–L957.
[18] H.A. Becerril, R.M. Stoltenberg, C.F. Monson, A.T. Woolley, J. Mater. Chem. 14 (2004) 611–616.
[19] J. Richter, M. Mertig, W. Pompe, I. Mönch, H.K. Schackert, Appl. Phys. Lett. 78 (2001) 536–538.
[20] M. Mertig, L.C. Ciacchi, R. Seidel, W. Pompe, Nano Lett. 2 (2002) 841–844.
[21] Y. Sakamoto, A. Fukuoka, T. Higuchi, N. Shimomura, S. Inagaki, M. Ichikawa, J. Phys. Chem. B 108 (2004) 853.
[22] J.C. Garno, Y. Yang, N.A. Amro, S. Cruchon-Dupeyrat, S. Chen, G.-Y. Liu, Nano Lett. 3 (2003) 389–395.
[23] T. Teranishi, A. Sugawara, T. Shimizu, M. Miyake, J. Am. Chem. Soc. 124 (2003) 4210–4211.
[24] Z.M. Fresco, J.M. Fréchet, J. Am. Chem. Soc. 127 (2005) 8302–8303.
[25] S. Krämer, R.R. Fuierer, C.B. Gorman, Chem. Rev. 103 (2003) 4367–4418.
[26] H. Sugimura, N. Nakagiri, Langmuir 11 (1995) 3623–3625.
[27] J. Zheng, Z. Zhu, H. Chen, Z. Liu, Langmuir 16 (2000) 4409–4412.
[28] Q. Li, J. Zheng, Z. Liu, Langmuir 19 (2003) 166–171.
[29] (a) Y. Masuda, T. Itoh, K. Koumoto, Langmuir 21 (2005) 4478–4481; (b) Y. Masuda, K. Tomimoto, K. Koumoto, Langmuir 19 (2003) 5179–5183.
[30] B. Cabot, A. Foissy, J. Mater. Sci. 33 (1998) 3945–3952.
[31] T. Yonezawa, H. Genda, K. Koumoto, Chem. Lett. 32 (2003) 194–195.
[32] N. Shirahata, Y. Masuda, T. Yonezawa, K. Koumoto, Langmuir 18 (2002) 10379–10385.
[33] H. Sugimura, N. Saito, N. Maeda, I. Ikeda, Y. Ishida, K. Hayashi, L. Hong, O. Takai, Nanotechnology 15 (2004) S69–S75.
[34] N. Shirahata, A. Hozumi, T. Yonezawa, Chem. Rec. 5 (2005) 145–159.

Japanese Journal of Applied Physics
Vol. 47, No. 2, 2008, pp. 1389–1392

Easy Preparation of Stable Iron Oxide Nanoparticles Using Gelatin as Stabilizing Molecules

Tetsu YONEZAWA*, Keigo KAMOSHITA[1], Masayoshi TANAKA[1], and Takatoshi KINOSHITA[1†]

Department of Chemistry, School of Science, The University of Tokyo, Bunkyo-ku, Tokyo 113-0033, Japan
[1]*Department of Material Science and Technology, Graduate School of Engineering, Nagoya Institute of Technology, Showa-ku, Nagoya 466-8555, Japan*

(Received April 17, 2007; accepted June 18, 2007; published online February 15, 2008)

Iron oxide nanoparticles were prepared by adding $NaBH_4$ to aqueous solution of an Fe^{3+} salt in the presence of gelatin as the stabilizing reagent. The obtained nanoparticles are relatively unique and can be separated by centrifugation. They can be collected in the dried powder form by centrifugation and freeze-drying. Their structural properties analyzed by transmission electron microscopy, atomic force microscopy and X-ray diffraction, as well as their magnetic properties measured by a superconducting quantum interface device are discussed in this paper. [DOI: 10.1143/JJAP.47.1389]

KEYWORDS: gelatin, iron oxide, nanoparticle, TEM, AFM

1. Introduction

Recently, the use of various metal and metal oxide nanoparticles has been proposed owing to their specific properties.[1–3] Furthermore, their applications as nanomaterials in biology, electronics, photonics, and chemical reactions, for example, have also been the focus of much attention in modern technology. In order to prepare stable nanoparticles, in most cases, organic stabilizing molecules are introduced before the reduction of metal ions in order to effectively protect the nanoparticle surface.[4] Polymers[5] and surfactants,[6] as well as metal coordinating reagents,[7,8] have been applied to stabilize nanoparticles in order to prevent their secondary aggregation or precipitation. For example, reverse micelles have been proposed in order to obtain well-size-controlled copper nanoparticles. Artificial polymers, such as poly(vinyl pyrrolidone) and poly(vinyl alcohol), have been widely used as protective reagents for metal nanoparticle catalysts.[5] Metal coordinative reagents, such as thiols[7] and amines,[8] have also been extensively applied to obtain size-controlled nanoparticles as well as to functionalize the nanoparticle surface. Such functionalized nanoparticles have been applied particularly to chemical or biological sensors.[9] Polypeptides can also be good stabilizing reagents for nanoparticles. D,L-Lipoic-acid-terminated polypeptides can attach to a gold nanoparticle surface with Au–S bond formation.[10] Gelatin, which is a native polypeptide, has also been considered as an important natural protective reagent for nanoparticles since the era of Faraday.[11] Gelatin has been widely used as the dispersing matrix of silver halide nanoparticles for photography-related materials and also as a good stabilizing reagent for various nanoparticles.

Materials researchers have a continuing intensive interest in the magnetic properties of metal or metal oxide nanoparticles because such nanoparticles are promising candidates for high-density memories. Sun *et al.* proposed the liquid preparation of FePt nanoparticles.[12] Iwamoto *et al.* have recently reported the low-temperature preparation of fct-structured FePt nanoparticles stabilized by poly(vinyl pyrrolidone).[13] Bioapplications of magnetic nanoparticles are also an important issue in modern science and technology. Application to induction of hyperthermia of biological tissues has been intensively investigated[14] and many empirical studies of animals have been carried out in order to realize the therapeutic effect of magnetic nanoparticles on tumors.[15] For such a purpose, biofriendly magnetic nanoparticles are strongly demanded. Magnetites have been of great interest, not only for their fundamental properties attributed to their multivalent oxidation states, but also for their technological applications. A technique of easy preparation of magnetites from $Fe(CO)_5$ was proposed by Woo *et al.*,[16] but this technique needs a relatively expensive starting material [$Fe(CO)_5$] and toxic CO is generated during the preparation.

On the basis of the above considerations, we attempted to prepare iron oxide nanoparticles by $NaBH_4$ reduction of iron salts in the presence of gelatin. Even after reduction by $NaBH_4$, the obtained nanoparticles were detected as iron oxides. This can be attributed to the smallness of the nanoparticles obtained in this study and the alkaline condition generated by $NaBH_4$ addition. Measurements using a superconducting quantum interface device (SQUID) magnetometer revealed that these nanoparticles showed superparamagnetism.

2. Experimental Procedure

Water was purified using Milli-Q (>18 MΩ). Gelatin was obtained from Wako Pure Chemicals, Japan, and used without further purification. Other reagents were used as received. X-ray diffraction (XRD) was measured using Rigaku RINT 2200 (Cu Kα, 40 kV, 30 mA). Transmission electron microscopy (TEM) was carried out using Hitachi H-800 (acceleration voltage: 200 kV) or Hitachi HF-2000 [field emission type, acceleration voltage: 200 kV, equipped with an charge-coupled device (CCD) camera supplied from AMT company]. TEM samples were prepared by putting a drop of nanoparticle dispersions on a carbon-coated copper TEM grid (150 or 200 mesh) and it was dried under reduced pressure. Atomic force microscopy (AFM) of the nanoparticles was carried out with Digital Instrument Nanoscope IV equipped with a Nanoworld SSS-NCH-10 cantilever (silicon single crystal with cantilever length of 125 μm, spring constant of 42 N/m, and frequency of 320 kHz). AFM was carried out in the tapping mode. An AFM sample was prepared by putting a drop of the dispersion on a freshly cleaved mica substrate, and it was dried under atmospheric

*E-mail address: tetsu@chem.s.u-tokyo.ac.jp
†E-mail address: kinoshita.takatoshi@nitech.ac.jp

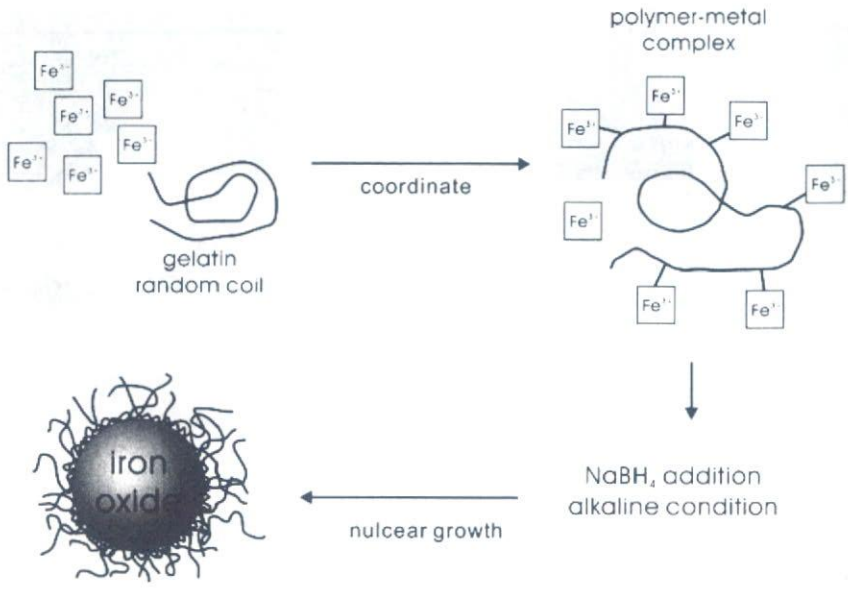

Fig. 1. Schematic illustration of preparation procedure of iron oxide nanoparticles stabilized by gelatin molecules.

pressure. Magnetic measurements were carried out using a Quantum Design MPMS-XL SQUID susceptometer under 100 Oe.

Gelatin-stabilized iron oxide nanoparticles were prepared by chemical reduction of iron(III) salts ($FeCl_3 \cdot 6H_2O$) in water. Under vigorous stirring, aqueous $NaBH_4$ (total amount, 115 mg in 5 cm^3 of water) was added dropwise to the aqueous solution (55 cm^3) of $FeCl_3$ and gelatin (100 mg) in a 100 cm^3 round-bottom flask at 50 °C. Hydrogen bubbles were generated during $NaBH_4$ addition. Nanoparticle dispersion occurred instantly. However, in some cases, dark brown precipitates were observed. The dispersions were sufficiently stable and no obvious color change was observed.

Isolation of gelatin-stabilized nanoparticles from dispersions was carried out by centrifugation. Aqueous nanoparticle dispersions were placed into centrifuge tubes, and then centrifuged for 9 h at 12000 rpm. The obtained nanoparticles were then freeze-dried for 12 h under vacuum in order to remove water molecules from the obtained nanoparticle powder. The powder was kept in a glass sample tube under ambient conditions.

3. Results and Discussion

The scheme of nanoparticle preparation is shown in Fig. 1. First, the gelatin and metal sauce mixture was introduced into the same flask. As gelatin has many metal coordination sites, such as methylthio ($-SCH_3$) groups and amino ($-NH_2$) groups, iron(III) ions should be coordinated with gelatin macromolecules to form polymer–metal complexes. This complex formation makes the reduction process mild and, as a result, smaller and more uniform nanoparticles can usually be obtained. For example, poly(vinyl pyrrolidone)-stabilized noble metal nanoparticles are relatively uniform and act as very effective catalysts.[2,13,17] The reaction temperature was 50 °C in order to change the molecular structure of gelatin from a helix to a random coil. The obtained nanoparticles were brownish. Sometimes, however, dark brown precipitates were generated after

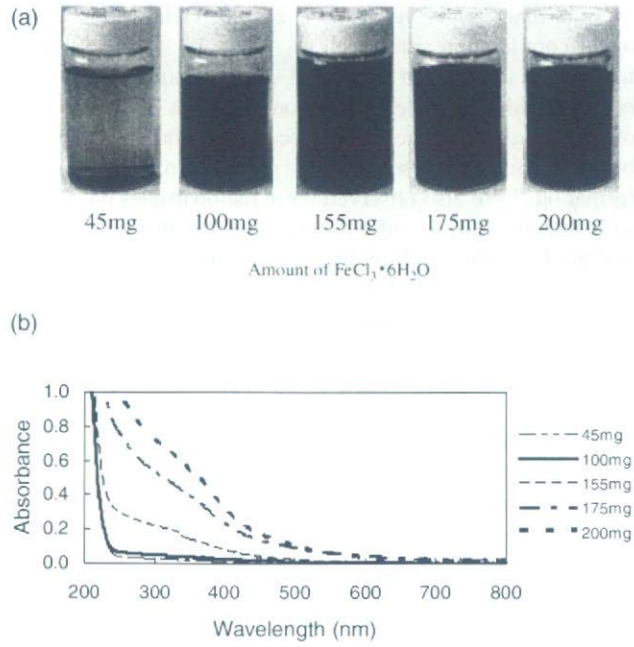

Fig. 2. (a) Images of the dispersion of gelatin-stabilized magnetic nanoparticles with various iron concentrations, and (b) UV–vis spectra of these dispersions.

reduction in the dispersion. The color of the obtained dispersion depended on the amount of iron salts. As clearly shown in Fig. 2(a), the color of the dispersion becomes darker with an increase in metal concentration. The UV–vis spectra of the obtained nanoparticle dispersions are shown in Fig. 2(b). In the less-than-450-nm region, absorption of the obtained nanoparticles is clearly indicated in these spectra. Shoulder absorption peaks can be observed at approximately 350 nm. A redshift in the absorption threshold is associated with an increase in particle size,[18] but no obvious shift can be observed in this figure.

A TEM image of the obtained nanoparticles and their size distribution are shown in Fig. 3. The obtained nanoparticles

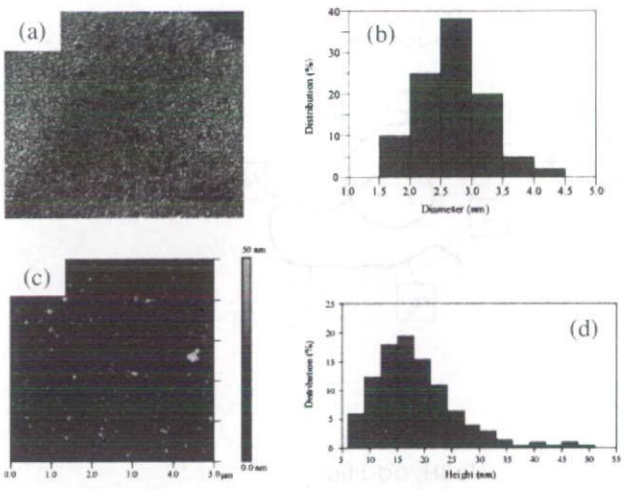

Fig. 3. (a) TEM image of gelatin-stabilized iron oxide nanoparticles and (b) their size distribution. (c) AFM image of gelatin-stabilized iron oxide nanoparticles placed on a graphite substrate and (d) the height distribution of particles ($FeCl_3 \cdot 6H_2O$: 175 mg).

are highly spherical and relatively unique in their size. The average diameter is very small, 2.8 nm. Gelatin has many metal coordination sites, such as $-NH_2$ and $-SCH_3$. Therefore, metal ion–gelatin and metal–gelatin complexes should be generated during the preparation processes. The reduction of metal ions and aggregation process of metal atoms should become mild because of this polymer–metal complex formation.[4] We also observed these nanoparticles on a solid substrate by AFM in order to determine the thickness of the organic layer surrounding the particle surface. The height of the obtained nanoparticles is about 18 nm. Not the width but the height of the particles obtained by an AFM probe study can be associated with the size of the nanoparticles containing an organic layer [Fig. 3(c)]. The height is the sum of twice of the thickness of the organic (gelatin) protective layer of the nanoparticles and the nanoparticle diameter. This technique is one of the most important techniques leading to the clarification of the structure and function of an organic stabilizing layer. Otherwise, the measurement of the diffusion coefficient[19] or a light-scattering method can be used for evaluating the size of nanoparticles with a stabilizing organic layer. However, in the case of using these measurement techniques, it is assumed that the nanoparticles are perfectly spherical. In the case of using the AFM technique, on the other hand, although the nanoparticles should be measured in dry form, one can evaluate each particle without any structural assumption.

The obtained nanoparticle dispersions were centrifuged in order to isolate the particles in the powder form, and to separate unbound (free) gelatin molecules. As the nanoparticles obtained here were extremely small, a high centrifugal force was required (12 000 rpm). After separation by centrifugation, the obtained sample was freeze-dried, because gelatin includes many water molecules in the surrounding polymer layer even after simple drying under vacuum, which produces flakes. The freeze-dry process yielded a brownish powder sample. Figure 4 shows a photograph of the obtained powder nanoparticles in a glass test tube and a 1.1 T rare-earth magnet was placed on the upper side of the test tube. As clearly noted in this figure, when a magnetic field was applied, the particles acquired a net magnetic moment and they were homogeneously attracted to the magnet. Figure 4 shows that these particles are magnetic.

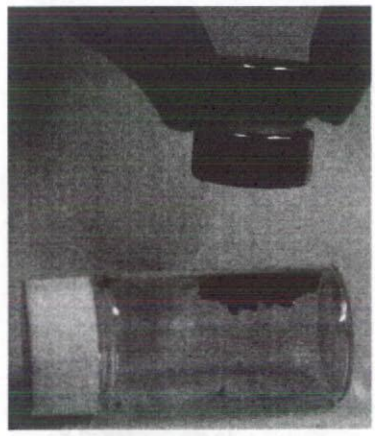

Fig. 4. Image of freeze-dried powder of iron oxide nanoparticles under a 1.1 T magnet ($FeCl_3 \cdot 6H_2O$: 175 mg).

An XRD pattern of the obtained nanoparticles is shown in Fig. 5. Cu Kα X-rays were irradiated onto the nanoparticle powder. Therefore, the XRD peaks are considerably broadened according to the size of the nanoparticles. On the basis of a comparison with the standard data, these nanoparticles can be considered as magnetite (Fe_3O_4) and maghemite (γ-Fe_2O_3). Magnetite and maghemite have similar XRD patterns, but the peak tops extracted from the obtained pattern [Fig. 5(b)] are identical to those of maghemite. Iron oxide nanoparticles prepared by thermal decomposition of $Fe(CO)_5$ with an average diameter of 5 nm were also considered to be maghemite.[16] Therefore, no effective reduction of Fe^{3+} to Fe^{2+} was observed even following the addition of a strong reducing reagent, $NaBH_4$, to form iron oxide particles.

Figure 6(a) shows the hysteresis curve of the obtained iron oxide nanoparticles stabilized by gelatin. Figure 6(b) shows the zero field cooling (ZFC) curve of the iron oxide nanoparticles recorded by a SQUID magnetometer. Coercivity and remanence are not detectable at 2 K, indicating superparamagnetic behavior. The magnetization at 2 K is about 58 emu g^{-1}. The magnetization of the ZFC curve of the iron oxide nanoparticles decreases gradually with temperature and indicates that these nanoparticles are superparamagnetic with some interactions among themselves. As these nanoparticles are superparamagnetic, they do not retain their magnetism after the removal of a magnet.

As gelatin is one of the fundamental biopolymers, these iron oxide nanoparticles should be highly biocompatible. Furthermore, gelatin-stabilized nanoparticles possess many useful functional groups, such as $-NH_2$ or $-COOH$, with which one can add various sensing groups or other functional molecules to the magnetic nanoparticle surface. Therefore, the process described here can be an easy method of preparing such useful nanoparticles.

4. Conclusions

We have described that the addition of aq. $NaBH_4$ to

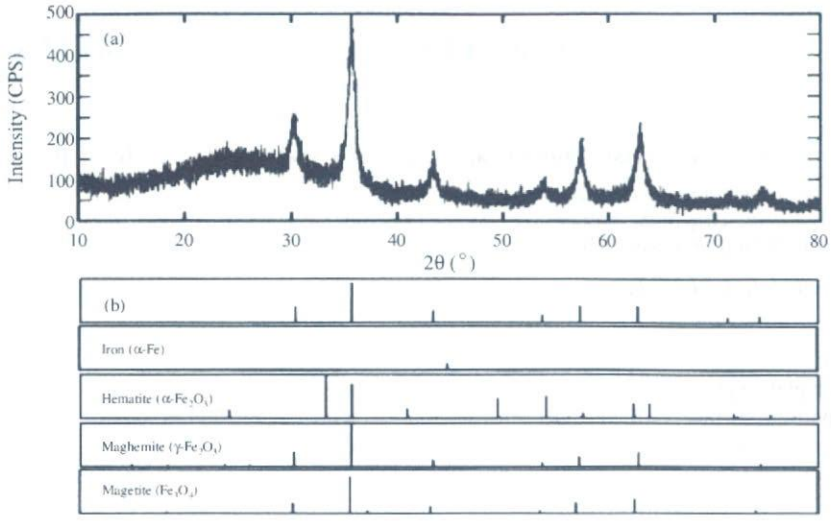

Fig. 5. (a) XRD pattern of iron oxide nanoparticles stabilized by gelatin. (b) Diffraction peaks extracted from pattern in (a) ($FeCl_3 \cdot 6H_2O$: 175 mg).

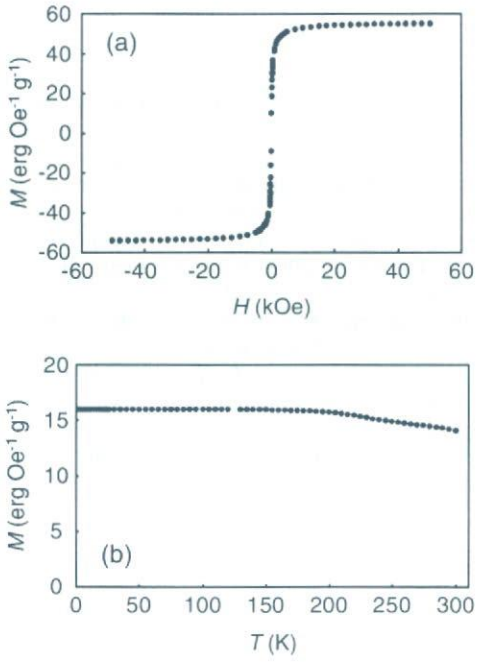

Fig. 6. (a) Hysteresis curve and (b) ZFC curve of the obtained iron oxide nanoparticles ($FeCl_3 \cdot 6H_2O$: 175 mg).

$FeCl_3$ aqueous solutions in the presence of gelatin in water provided stable iron oxide nanoparticles. The obtained iron oxide nanoparticles are relatively small (2.8 nm diameter), and surrounded by a thick gelatin layer, which well stabilizes these particles in water. The thickness of the gelatin layer was estimated to be 7.6 nm by AFM. SQUID measurements revealed that these nanoparticles were superparamagnetic and can be applied as biomaterials.

Acknowledgements

The authors thank Dr. W. Fujita of Nagoya University and Mr. M. Tomonari of ISK for their assistance in the experiments. TY thanks Professors H. Nishihara (University of Tokyo) and F. Watari (Hokkaido University) for their warm hospitality during the completion of this work. The authors thank the Japan Aerospace Exploration Agency (JAXA) for the partial financial support. TY also is thankful for the partial financial support from Health and Labour Sciences Research Grants for Research on Risk Assessment of Chemical Substances: "Development of Visualization Method of Dynamical Motion Behavior of Nanoparticles in the Internal Body (H18-Chem-General-006)" from the Ministry of Health, Labour and Welfare.

1) *Nanoparticles*, ed. G. Schmid (Wiley-VCH, Weinheim, 2004).
2) T. Yonezawa: in *Morphology Control of Materials and Nanoparticles*, ed. Y. Waseda and A. Muramatsu (Springer, New York, 2004) p. 85.
3) *Colloids and Colloid Assemblies*, ed. F. Caruso (Wiley-VCH, Weinheim, 2004).
4) T. Yonezawa and N. Toshima: in *Advanced Functional Molecules and Polymers*, ed. H. S. Nalwa (Overseas Publishers Association, Amsterdam, 2001) Vol. 2, Chap. 3, pp. 65–86.
5) M. P. Pileni: J. Phys.: Condens. Matter **18** (2006) S67.
6) N. Toshima and T. Takahashi: Bull. Chem. Soc. Jpn. **65** (1992) 400.
7) M. Brust, M. Walker, D. Bethell, D. J. Schiffrin, and R. Whyman: J. Chem. Soc., Chem. Commun. (1994) 801.
8) Y. Negishi, Y. Takasugi, S. Sato, H. Yao, K. Kimura, and T. Tsukuda: J. Phys. Chem. B **110** (2006) 12218.
9) H. Otsuka, Y. Akiyama, Y. Nagasaki, and K. Kataoka: J. Am. Chem. Soc. **123** (2001) 8226.
10) T. Yonezawa, T. Nomura, T. Kinoshita, and K. Koumoto: J. Nanosci. Nanotechol. **6** (2006) 1649.
11) M. Faraday: Philos. Trans. R. Soc. London **147** (1847) 145.
12) S. Sun, C. B. Murray, D. Weller, L. Folks, and A. Moser: Science **287** (2000) 1989.
13) T. Iwamoto, K. Matsumoto, Y. Kitamoto, and N. Toshima: J. Colloid Interface Sci. **308** (2007) 564.
14) A. Ito, M. Shinkai, H. Honda, and T. Kobayashi: J. Biosci. Bioeng. **100** (2005) 1.
15) J. K. Räty, T. Liimatainen, T. Wirth, K. J. Airenne, T. O. Ihalainene, T. Huhtala, E. Hamerlynck, M. Vihinen-Ranta, A. Närvänen, S. Ylä-Herttuala, and J. M. Hakumäki: Gene Ther. **13** (2006) 1440.
16) X. K. Woo, J. Hong, S. Choi, H.-W. Lee, J.-P. Ahn, C. S. Kim, and S. W. Lee: Chem. Mater. **16** (2004) 2814.
17) N. Toshima, T. Yonezawa, and K. Kushihashi: J. Chem. Soc., Faraday Trans. **89** (1993) 2537.
18) N. Nassar and M. Husein: Phys. Status Solidi A **203** (2006) 1324.
19) T. Yonezawa, T. Tominaga, and N. Toshima: Langmuir **11** (1995) 4601.

Platinum Nanoflowers for Surface-Assisted Laser Desorption/Ionization Mass Spectrometry of Biomolecules

Hideya Kawasaki,[†] Tetsu Yonezawa,*[,‡] Takehiro Watanabe,[†] and Ryuichi Arakawa*[,†]

Department of Applied Chemistry, Faculty of Engineering, Kansai University, 3-3-35, Yamate-cho, Suita, Osaka 564-8680, Japan, and Department of Chemistry, Graduate School of Science, The University of Tokyo, 7-3-1 Hongo, Bunkyo-ku, Tokyo 113-0033, Japan

Received: July 3, 2007; In Final Form: August 28, 2007

No-template synthesis of surface clean platinum nanomaterials with thin projections (petals) on the Pt nanoparticle surface, termed Pt nanoflowers, has been developed, and Pt nanoflowers have achieved superior performance on surface-assisted laser desorption/ionization mass spectrometry (SALDI−MS) of biomolecules. With this new material, one can obtain high-resolution mass spectra with lower laser energy and smaller sample amounts, and no organic matrix is needed for laser desorption/ionization. The mass spectra also have fewer obstacle peaks at the lower *m/z* region. Furthermore, this novel substrate is quite stable against aging and showed no sweet-spot problems, that is, equal sensitivity on the whole substrate surface. Various biomolecules, including peptides and phospholipids, were examined, and Pt nanoflowers showed good performance for matrix-free laser desorption/ionization MS of these materials.

Introduction

Metal particles with nanometer-scale dimensions are of great interest due to their unusual properties.[1−2] The size and shape-dependent physicochemical and optoelectronic properties of metal nanoparticles have important applications in catalysis and biosensing, recording media, and optics. Recently, gold and silver nanoparticles, which display specific strong surface plasmon absorption properties, have been used in various analytical techniques such as biological optical imaging,[3] bio-(chemical)sensing applications,[4] and surface-enhanced Raman scattering.[5]

Matrix-assisted laser desorption/ionization mass spectrometry (MALDI-MS) has become a powerful tool for the analysis of biomolecules and synthetic polymers.[6−10] In MALDI-MS, analyte compounds are embedded in a surplus of matrix, consisting of small organic molecules with strong absorbance at the laser wavelength used, and are codesorbed upon laser excitation. Although MALDI-MS has been successfully applied to the analysis of biomolecules and synthetic polymers, it has not been extensively used for low molecular-weight compounds (<500), due to the relatively high intensity of the background signals of the organic matrices in the low-mass range. In addition, the inhomogeneous cocrystallization of analytes with a matrix, such as 2,5-dihydroxybenzoic acid (DHB), requires sweet-spot searching, which leads to poor shot-to-shot and sample-to-sample reproducibility.

In the past few years, various nanomaterials such as graphite,[11] carbon nanotubes (CNT),[12] porous silicones,[13−15] TiO_2 nanoparticles,[16] and gold nanoparticles[17] have received attention for their utility in surface-assisted laser desorption/ionization mass spectrometry (SALDI-MS)[18] employing these inorganic substrates because of the high surface areas of nanoparticles, simple sample preparation techniques, flexibility, and selectivity of sample deposition. Russell et al. have demonstrated that size-selected gold nanoparticles (2−10 nm diameters) can be used as SALDI-MS under dry surface conditions for the detection of peptides such as substance P and phosphopeptides, although abundant ions from the Au clusters appear in the mass spectra.[19] Nanoparticles are usually prepared in the presence of stabilizing reagents, that is, polymers, surfactants, or metal coordinative ligands.[20,21] However, such stabilizing reagents may afford to decrease the effectiveness of SALDI-MS. That is, mass peaks from stabilizing reagents themselves, which coat the particle surface, become obstacle signals instead of those from organic matrix molecules. In practice, Tseng et al. reported that bare Au nanoparticles without stabilizing reagents offer some advantages in terms of high ionization efficiency and quantitative improvement in the analysis of small carbohydrates.[22]

Platinum is very stable and is not easily oxidized under ambient atmospheric conditions. The nanosized platinum is black in color and can therefore be used as a SALDI-MS matrix for any laser wavelength. Moreover, the fragmentation from metal nanoparticles such as Au clusters can be diminished because Pt has a very high-melting temperature (2045 K), high crystallinity, and a relatively low-thermal conductivity value (71.6 W m^{-1} K^{-1} at 300 K). Further, platinum nanoparticles are black and are able to effectively adsorb laser beam all over the UV−vis region. Therefore, Pt should be a good candidate substrate for SALDI-MS. However, to date, no attempts have been made to apply Pt nanoparticles to analytical techniques of SALDI-MS. Herein, we for the first time have developed the stabilizing reagent−free synthesis of Pt nanomaterials with thin projections on the Pt nanoparticle surface, termed Pt nanoflowers, and demonstrated the effectiveness of mass spectrometric applications of easily prepared Pt nanoflowers. The specific structure of Pt nanoflowers was observed by high-resolutioin electron microscopy (HR-EM), and this "flowerlike" structure with thin petals on the surface was shown to yield good performance on SALDI-MS of peptides and lipids. This

* To whom correspondence should be addressed. E-mail: (R.A.) arak@ipcku.kansai-u.ac.jp; (T.Y.) tetsu@chem.s.u-tokyo.ac.jp.
† Kansai University.
‡ The University of Tokyo.

10.1021/jp075159d CCC: $37.00
Published on Web 10/10/2007

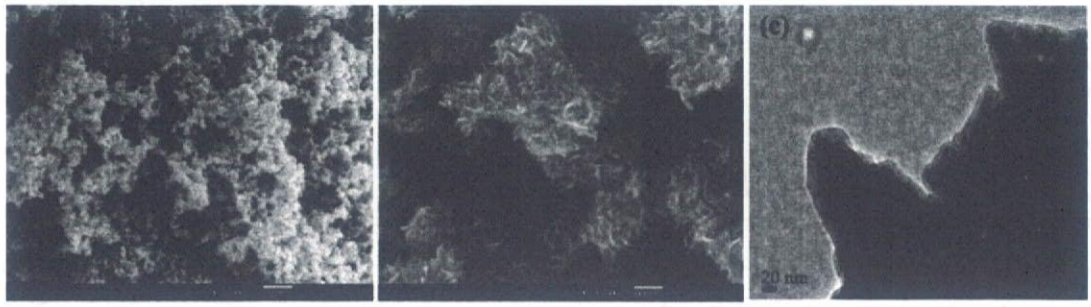

Figure 1. HR-SEM images of Pt nanoflower at magnifications of (a) 10 000 and (b) 100 000. (c) HR-TEM image of the same Pt nanoflowers. White lines in HR-SEM images indicate the platinum thin projections (petals) of Pt nanoflowers. These white lines correspond to the gray.

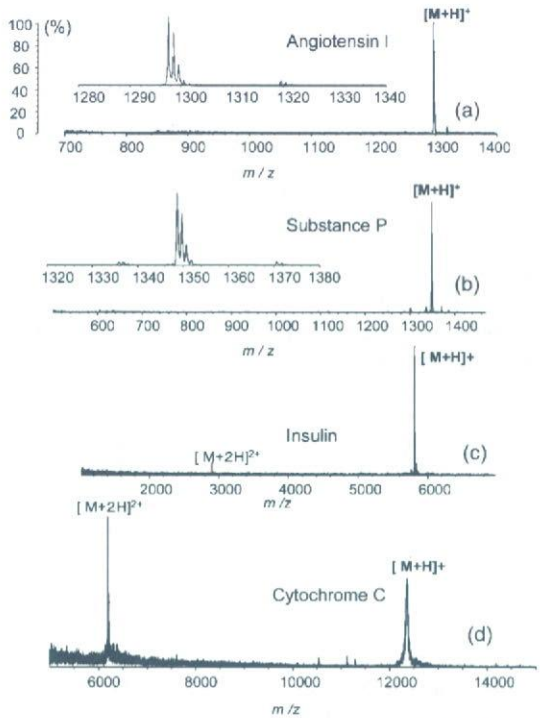

Figure 2. The mass spectra of (a) angiotensin I (500 fmol), (b) substance P (500 fmol), (c) human insulin (800 fmol), and (d) cytochrome C (5 pmol) obtained from Pt nanoflowers as the SALDI-MS.

flowerlike specific structure may play an important role to desorption/ionization of the samples.

Experimental Section

Materials. Metal sources for platinum nanoflowers, that is, hexachloroplatinum(IV) acid ($H_2PtCl_6 \cdot 7H_2O$) obtained from Kojima Chemical Co. or Kanto Chemical (Tokyo, Japan). 1,2-Dimyristoyl-sn-Glycero-3-Phosphocholine (DMPC) and 1,2-Dioleyl-sn-Glycero-3-Phosphocholine (DOPC) were obtained from Avanti Polar Lipids Inc., and 1,2-dilauroyl-sn-Glycero-3-Phosphocholine (DLPC) and 1,2-Dipalmitoyl-sn-Glycero-3-Phosphocholine (DPPC) were obtained from NOF Corporation, Japan. Angiotension I and substance P were purchased from Wako Pure Chemical Co. All other chemicals were purchased from Wako Pure Chemical Co.

Preparation of Pt Nanoflowers. The Pt source, $H_2PtCl_6 \cdot 7H_2O$ (1 g, 1.95 mmole) was dissolved in 150 cm^3 of deionized water. Under vigorous stirring, the reductant ($NaBH_4$, 380 mg, 10 mmole) was introduced all at once into this aqueous solution.[23] An abundance of hydrogen bubbles was generated and the clear yellow solution immediately turned black. The black dispersion was continuously stirred for several hours. Black precipitates were then collected over a hydrophilic poly-(tetrafluoroethylene) (PTFE) membrane filter with a pore size of 200 nm (Advantec-Toyo, Japan). The black powder obtained here was washed with pure water several times to eliminate free ions, for example, Na^+, unreduced $PtCl_6^{2-}$, BO_3^{2-}, etc. The pure Pt nanoflowers were then dried under vacuum conditions for > 12 h at room temperature. The dried powder was kept in the ambient atmosphere in a glass tube. We also prepared spherical Pt nanoparticles for SALDI-MS. The same synthetic process used for the Pt nanoflowers was employed for the Pt nanoparticles, except that the solution of reductant ($NaBH_4$, 380 mg in 10 mL of water, 10 mmol) was introduced by dropwise addition into the aqueous solution of H_2PtCl_6 for the slow reduction of Pt ions.

Preparation of Pt-Coated Silicon Substrates. Platinum thin films were coated on a silicon wafer by using a MSP-10 magnet sputter (Vacuum Device, Japan). The thickness of the platinum film is 10−40 nm.

SALDI-MS Analysis with Pt Nanoflowers. The two layer sample preparation method was employed for SALDI-MS of biomolecules with Pt nanoflowers: the first step was spotting of the Pt nanoflower solution (1 μL, 15 mg/ mL), prepared by dispersing Pt nanoflowers in pure water with ultrasonication for 5 min on a stainless steel plate, followed by drying; the second step was typically deposition of a 0.5 μL sample solution on the plate. For peptides, the sample aqueous solution was mixed with a citrate aqueous solution [triammonium citrate (50 mM)/citric acid (100 mM), 3:1 (v/v)] for SALDI-MS analysis, according to the method of Chen et al.[24] For lipids, the first step was spotting of the Pt nanoflower solution (1 μL) onto a stainless steel plate, followed by deposition of the citrate aqueous solution (1 μL). The lipids (0.5 μL, 0.25 mg /mL) in chloroform solvent were then deposited on top of the Pt nanoflowers treated with the citric buffer.

Instrumentation. Mass spectra were acquired in both positive reflectron and linear mode using an AXIMA-CFR time-of-flight mass spectrometer (Shimadzu/Kratos, Manchester, UK) with a pulsed nitrogen laser (337 nm). A 1 μL drop of the aqueous dispersion of Pt nanoflowers was placed on a Si wafer, and its surface was observed by scanning electron microscopy (SEM) (JEOL JSM-7401FNT) at 15 kV before and after laser irradiation in an AXIMA-CFR with a regular laser desorption/ionization mass spectrometry LDI-MS condition. Transmission electron microscopy (TEM) images of the nanoflowers were taken with a Hitachi HF-2000 with an acceleration voltage of 200 kV. A drop of the dispersion of Pt nanoflower was put on a carbon-coated Cu grid.

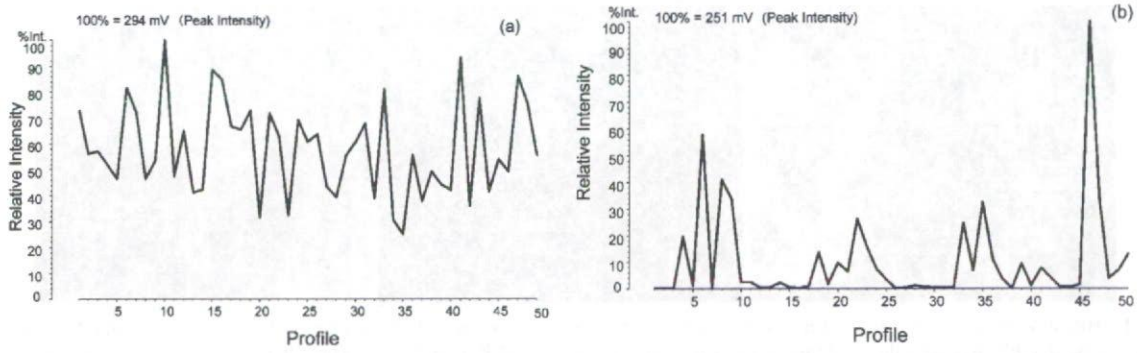

Figure 3. Plot of relative peak intensities of angiotensine I (500 fmol) obtained from 50 different sample spots in SALDI-MS with (a) Pt nanoflowers and (b) DHB matrix (15 mg/mL). The conditions for Pt nanoflowers were the same as those in Figure 2. In the case of DHB, the sample data were collected at the edges of the sample, which might be sweet-spot positions.

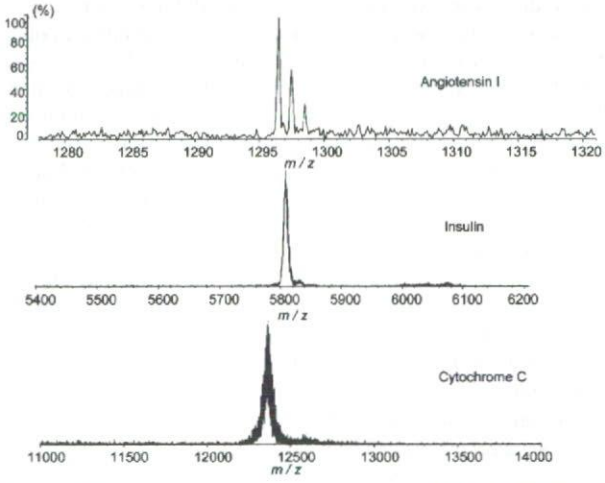

Figure 4. The mass spectra of (a) angiotensin I (0.7 fmol), (b) human insulin (5 fmol), and (c) cytochrome C (20 fmol) obtained from Pt nanoflowers for SALDI-MS.

Results and Discussion

Pt Nanoflower Characterization. As described above, the fundamental properties (high-melting temperature, low-thermal conductivity, very high stability, and adsorption property of laser beam) of platinum make it highly suitable as a substrate for SALDI-MS. However, to obtain high sensitivities in SALDI-MS, the nano-Pt surface must be without organic contamination, which gives background noise signals, especially in a lower *m/z* region. This would necessitate the creation of a novel preparation process for nano-Pt use in SALDI-MS. Very severe reduction conditions were applied to prepare Pt nanoflowers in this study. A large excess of $NaBH_4$ was injected at one time into the $PtCl_6^{2-}$ aqueous solution. $NaBH_4$ instantly decomposes in the aqueous solution to give hydrogen and $NaBO_2$. Decomposition of $NaBH_4$ is very fast in an acidic condition, and a great abundance of hydrogen bubbles was generated in this preparative step.

Figure 1a,b are HR-SEM images of Pt nanoflowers at magnifications of 10 000× and 100 000×. A drop of the aqueous dispersion was placed on a doped Si wafer, and the sample was dried under vacuum conditions, as on the stainless sample plate of MALDI-MS for measurement. Aggregated structures were observed because no protective reagent was introduced during the preparation. As can be clearly seen in this SEM image, the Pt nanoflower has a very interesting structure. The Pt nanoflowers are not spherical but rather have numerous thin projections, resembling petals, which can be seen on the surface and give a flowerlike appearance. The HR-TEM image of Pt nanoflowers (Figure 1c) shows these projections on the nanoparticles to be very thin but relatively wide, just like petals of flowers. The contrast of nanosized Pt is usually very dark even though their size is in single nanometer level. However, as clearly shown in Figure 1c, the TEM contrast of Pt petals is very weak. This image suggests that the thickness of these petals is a few nanometers. We refer to these nano-Pt particles as Pt nanoflowers.

In contrast to the case of Pt nanoflowers, the reductant of $NaBH_4$ was introduced a little at a time into the aqueous solution of H_2PtCl_6 for the slow reduction of Pt ions. Slow addition of $NaBH_4$ gives secondary aggregates of small spherical platinum nanoparticles but no such petal was observed (Supporting Information, Figure S1). Slow addition of $NaBH_4$ did not give an abundance of hydrogen bubbles because $NaBH_4$ was added slowly, and also the pH value of the preparative solution becomes higher during the addition of $NaBH_4$. Decomposition of $NaBH_4$ is strongly affected by pH. It is reasonable to speculate that hydrogen bubbles generated during this fast reduction process play a very important role in generating these thin projections (petals) on the Pt nanoparticles.

Application of Pt Nanoflowers to SALDI-MS Analysis of Biomolecules. *Peptides.* Figure 2 a,b shows the mass spectra of angiotensin I and substance P, respectively, obtained from Pt nanoflowers during SALDI-MS. The insets in the figure are expanded views of the molecular ion region. Using Pt nanoflowers, we have successfully ionized angiotensin I (m/z =1298 Da) and substance P (1349 Da) in the proton adduct forms of $[M + H]^+$ in the mass spectra, and the isotope peaks of peptides were thus clearly resolved.

To examine the shot-to-shot reproducibility of signals in SALDI-MS with Pt nanoflowers, we collected the signal intensities from 50 different sample spots. Figure 3 shows that the signal peaks from angiotensin I are seen at any potions without the sweet spots typical of standard chemical matrices. For comparison, the shot-to-shot reproducibility of signals in MALDI-MS with DHB matrix is shown in the Figure 3b. The variability of the signal intensities of angiotensin I is relatively smaller than that with DHB matrix. Especially, no mute spot was observed. The average value (Av) and standard deviation (SD) for the peak intensities were as the follows: 61.0 (Av) and 14.4 (SD) for Pt nanoflowers and 11.6 (Av) and 18.2 (SD) for DHB. The sweet spot problem can be usually explained by the quality of mixed crystal of sample molecules and organic matrix molecules on the sample plate. In addition, organic matrices such as DHB have problems with precipitation that might occur at the edges of the sample due to inhomogeneous

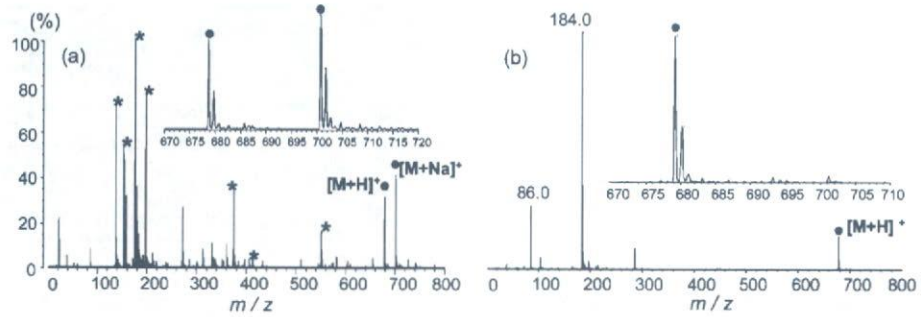

Figure 5. The mass spectra of DMPC (0.2 mg/mL, 0.5 mL) obtained from (a) DHB matrix for MALDI-MS and (b) Pt nanoflowers for SALDI-MS. Characteristic matrix signals are marked with asterisks.

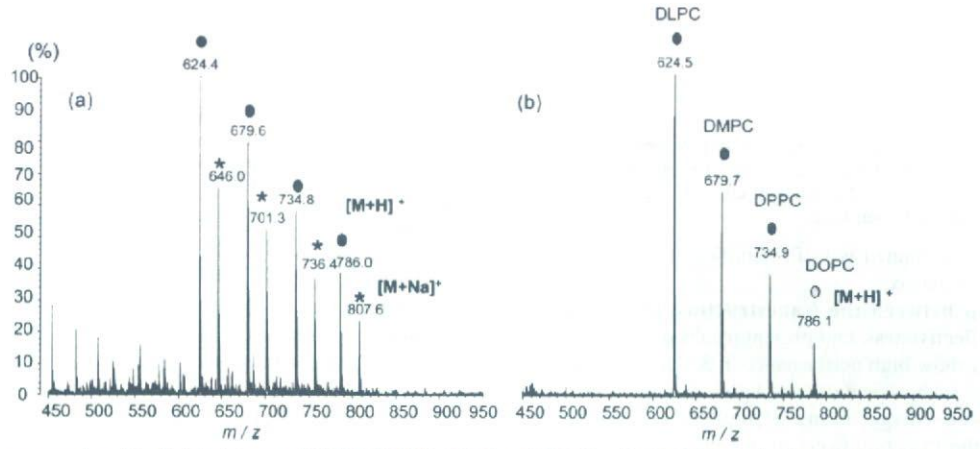

Figure 6. The mass spectra of the lipid mixtures of DLPC, DMPC, DPPC, and DOPC with (a) DHB matrix for MALDI-MS and (b) Pt nanoflowers for SALDI-MS.

solvent evaporation on the plate. In our system, no such good mixed crystal is needed for the performance of mass spectroscopy. This useful property of Pt nanoflowers for SALDI-MS can be explained also by the SEM image shown in Figure 1. Pt nanoflowers were aggregated on the sample plate but they were deposited on the wide area of the plate.

In addition, we have found that the Pt nanoflower can also successfully generate larger molecules such as insulin (5807 Da) and cytochrome C (12 360 Da), showing the single proton adduct forms of $[M + H]^+$ and double proton adduct form $[M + 2H]^{2+}$ in the MS spectrum (Figure 2c,d). The mass limit for this method might be at most about m/z 20 kDa because the peak of V8 Protease (~30 kDa) was not detected. The minimum amount of sample needed for obtaining spectra with reasonable signal-to-noise ratios for Pt nanoflowers was as low as 0.7 fmol for angiotensin I, 5 fmol for insulin, and 20 fmol for cytochrome C, as shown in Figure 4. These detection limits (~ a few femtomoles) of peptides were 100 times higher than those of peptides obtained using Au nanoparticles (~100 fmol).[19] The performance of Pt nanoflowers used as the SALDI matrix is similar to that of Fe_3O_4/TiO_2 nanoparticles.[25] The specific structure of Pt nanoflowers may play an important role for this high sensitivity. Usually, polymers can be adsorbed onto inorganic surfaces at many points. Therefore, the detachment of a polymer molecule from the surface is significantly difficult and needs very high energy, even the interaction between a polymer unit and the surface is very small. On the other hand, the petals on these platinum nanoflowers are very thin, and it can be speculated that the number of adsorption points is smaller compared with a flat surface. This unique structure of Pt nanoflowers gives the higher sensitivity and the better quality of the mass peaks of biopolymers. Such specific properties of Pt nanoflowers according to their structure will be discussed later.

Phospholipids. The analysis of phospholipids is an ever-expanding field due to the importance of these molecules in biochemistry as well as industry. MALDI-MS with chemical matrices has been developed for the analysis of lipids and phospholipids.[10] Compared to the use of a conventional chemical matrix of DHB (Figure 5a), the Pt nanoflower indicated that there is few number of degradation species from the molecular ion (m/z = 680) of DMPC, and signals were isotopically resolved, as shown in Figure 5b. The Pt nanoflower required much lower laser fluence: the minimum laser power needed to detect a molecular ion with the use of Pt nanoflowers was about half than that of DHB matrix, which is probably attributable to their numerous thin and wide surface projections. As a result, the species from degradation reactions were barely detectable, although the fragments (m/z 184 and 86) from the polar head group were still present. One of the most challenging problems in MALD-MS analysis is characterization of multicomponent mixtures like peptides and lipids. The SALDI-MS spectra of the lipid mixtures of DLPC, DMPC, DPPC, and DOPC with Pt nanoflowers demonstrate that the corresponding molecular ions $[M + H]^+$ of the lipids are easily identified even in lipid mixtures above m/z >500 (Figure 6b), as compared to the complex MALDI-MS spectrum of lipid mixtures obtained using the DHB matrix (Figure 6a). Thus, the use of Pt nanoflowers is preferable for SALDI-MS analysis of lipids, and the quality of

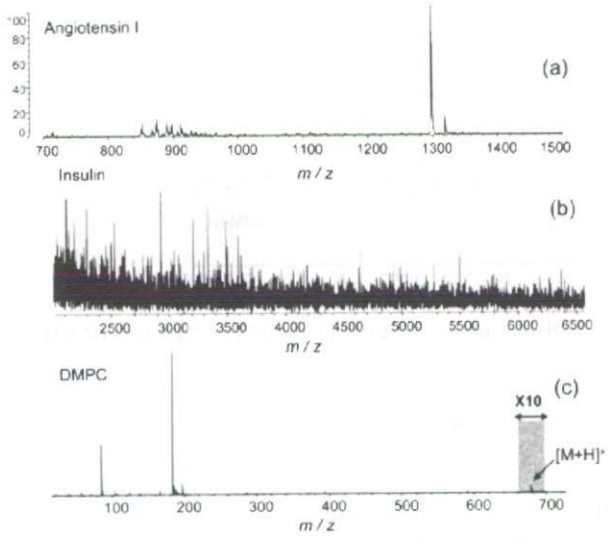

Figure 7. The mass spectra of (a) angiotensin I (5 pmol), (b) human insulin (5 pmol), and (c) DMPC (0.2 mg/mL, 0.5 mL) obtained from SALDI−MS with spherical Pt nanoparticles. The peak intensity, $[M + H]^+$ is expanded by ten times.

the mass spectra obtained with Pt nanoflowers is superior to that of the DHB matrix.

Relationship between the Nanostructure of Pt and the SALDI-MS Effectiveness. Our present results demonstrate that Pt nanoflowers show high performance in SALDI-MS analysis of biomolecules such as peptides and lipids. Pt nanoflowers can efficiently absorb energy during desorption, and the energy transfer from the Pt nanoflowers to the analytes likely would occurs via a thermally driven process, inducing the laser desorption/ionization of alalytes, as similar to the mechanism proposed by Tanaka.[6] Here, we consider the important factors of the nanostructure of Pt nanoflowers in SALDI-MS. To examine the relationship between the nanostructure of Pt and the SALDI-MS effectiveness, we performed the SALDI-MS of peptides and lipids also with spherical Pt nanoparticles. We found that the spherical Pt nanoparticles can also generate molecular ion of angiotensin I $[M + H]^+$ (Figure 7a), but the larger molecular ion of insulin was not detected in the MS spectrum (Figure 7b). In the case of DMPC, the fragments (m/z 184 and 86) from the polar head group were dominantly present, and hence the soft ionization of the lipid was difficult with the use of spherical Pt nanoparticles (Figure 7c). These results indicate that the characteristic morphology of Pt nanoflowers is effective in extending the mass range and the soft ionization. In addition, we also prepared Pt-coated silicon substrates for SALDI-MS by spattering of Pt at surface thicknesses of 10, 20, 30, and 40 nm. However, the mass spectra of angiotensin I with Pt-coated silicons were far worse in terms of sensitivity, as compared to Pt nanoflowers (Supporting Information, Figure S2). The Pt-coated silicons required much higher laser fluence to detect the molecular ion, which was about two times higher than that of Pt nanoflowers.

From the above results, it is reasonable to conclude that Pt nanoflowers cannot only efficiently absorb energy during desorption, but morphological features of Pt nanoflowers such as the roughness and porosity generated by the formation of petals as well as the tip sharpness of the petals on the surface are very important in lowering detection limits and in extending the mass range. Dense arrays of single-crystal silicon nanowires with tip sharpness have been used as a platform for LDI-MS of peptides.[26] The feature of the nanowire surface produced lower

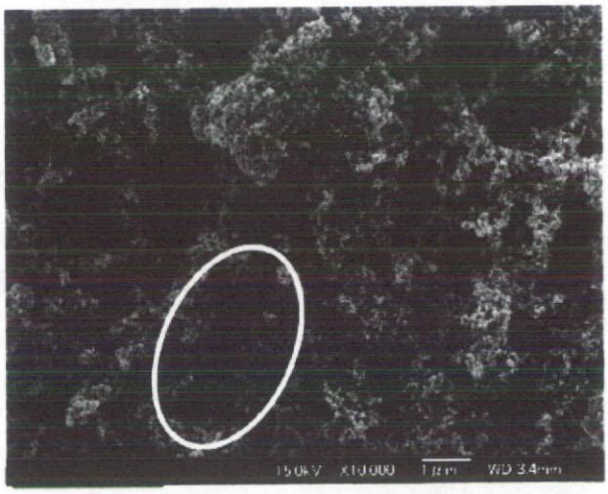

Figure 8. HR-SEM images of the surface of the Pt nanoflower SALDI-MS plates after laser irradiation.

laser energy as compared to porous silicon and MALDI to desorb/ionize small molecules, therefore reducing background ion interference. The same may be said of Pt nanoflowers with tip sharpness. Larger molecules have more adsorption points on the surface of inorganic materials, and this makes it much more difficult for the molecules to be detached from the surface by laser energy because all adsorption points should be separated at the same time. It can be readily understood that macromolecules need higher laser power than small molecules to be detected in SALDI-MS. But a lower laser power for desorption was strongly desired to avoid the formation of fragment ions. Further, in particular, the projections on Pt nanoflowers can act as tiny antennas producing significant field enhancement in the vicinity of the nanometer sharp tip.[26,27] Further control of physical dimensions of Pt nanoflowers such as porosity, tip sharpness, and density would offer greater potentials for the SALDI of biomolecules.

Effect of Laser Irradiation on Pt Nanoflower SALDI-MS Plates. Even though platinum has a very high melting point, deformation or ablation of platinum nanostructure may occur during the irradiation of a pulse laser. In nanodimension, melting temperature of metals becomes lower than bulk metals.[28] Thus, we have compared the structure of platinum nanoflowers before and after mass spectroscopic observation. Figure 8 shows a HR-SEM image of the surface of the Pt nanoflower SALDI-MS plates after laser irradiation. In the center of the image, a small flat space or a narrow but flat line is observed, as denoted by a circle. During the observation of mass spectroscopy, one often scans the laser beam on the sample plate. This caused the flat line as shown in Figure 8. The width of the flat line is ca. 500 nm, which is much narrower the laser beam spot radius. This is probably due to the high stability and the high melting temperature and the stability of Pt.

Conclusion

Development of nanomaterials with unique optical, thermal, and electric properties into conventional analytical tools has fundamentally changed bioanalytical measurements in recent decades. We have demonstrated the no-template synthesis of surface clean platinum nanomaterials with thin projections on the Pt nanoparticle surface, termed as Pt nanoflowers, for SALDI-MS for the first time. With this new material, one can obtain high sensitivity with lower laser energy and smaller